

CoMFA based *de novo* design of Pyrrolidine Carboxamides as Inhibitors of Enoyl Acyl Carrier Protein Reductase from *Mycobacterium tuberculosis*

Ashutosh Kumar · Mohammad Imran Siddiqi

Received: 13 February 2008 / Accepted: 29 May 2008 / Published online: 15 July 2008
© Springer-Verlag 2008

Abstract InhA, the enoyl acyl carrier protein reductase (EACP reductase) from *Mycobacterium tuberculosis*, is one of the key enzymes involved in the mycobacterial fatty acid elongation cycle and has been validated as an effective target for the development of anti-microbial agents. We report here, comparative molecular field analysis (CoMFA) studies and subsequent *de novo* ligand design using the LeapFrog program on pyrrolidine carboxamides, which have been reported as selective inhibitors of EACP reductase from *Mycobacterium tuberculosis*. The CoMFA model, constructed from the inhibitors used in this study has been successfully used to rationalize the structure-activity relationship of pyrrolidine carboxamides. The CoMFA model produced statistically significant results with cross-validated and conventional correlation coefficients of 0.626 and 0.953 respectively. Further, the predictive ability of CoMFA model was determined using a test set which gave predictive correlation coefficient r^2_{pred} of 0.880, indicating good predictive power. Finally, Leapfrog was used to propose 13 new pyrrolidine carboxamide analogues, based on the information derived from the CoMFA contour maps. The designed molecules showed better predicted activity using the CoMFA model with respect to the already reported systems; hence suggesting that newly proposed molecules in this series of compounds may be more potent and selective toward EACP reductase inhibition.

Keywords Antitubercular agents · CoMFA · Pyrrolidine Carboxamides · 3D-QSAR

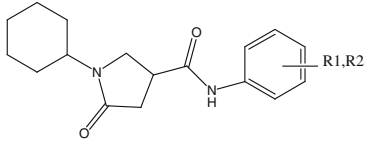
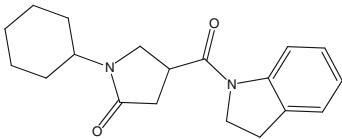
Introduction

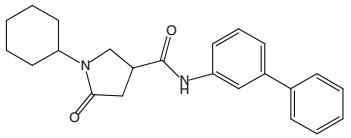
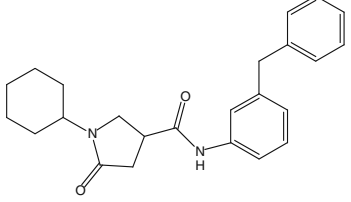
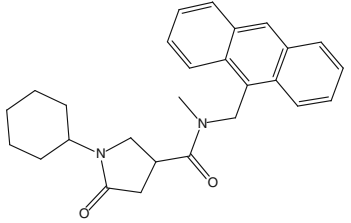
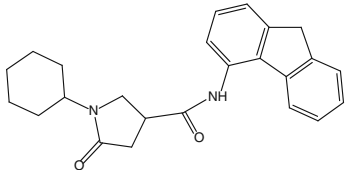
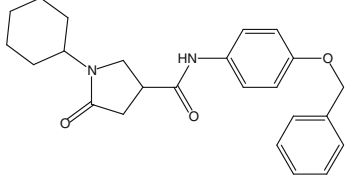
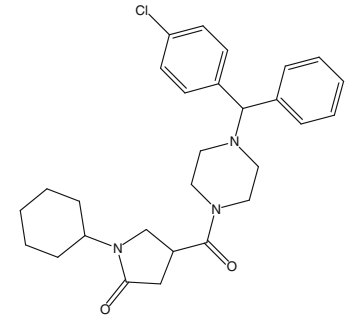
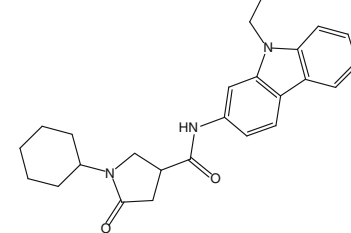
Tuberculosis is the leading cause of mortality from a single infectious agent and is responsible for more than 2 million deaths worldwide every year [1]. Current control efforts are severely hampered by the fact that *Mycobacterium tuberculosis* (MTB) is a leading opportunistic infection in patients with AIDS and by the spread of multidrug-resistant strains of MTB (MDRTB) [2–5]. Over the decade, it is estimated that as many as 50 million people worldwide have been infected with MDRTB strains. According to WHO, from 2002 to 2020, there will be about 1 billion more people newly infected with TB and approximately 36 million deaths if the worldwide ravage of tuberculosis is left unchecked [1]. Despite the increasing worldwide incidence of TB and its alarming threat toward public health, no novel antituberculosis drugs have been introduced into clinical practice over the past four decades. Therefore there is an imperative need to develop novel antitubercular drugs for the management of tuberculosis, i.e., having new mechanism of action and also will be able to minimize the chances of MDR strains with shorter duration of therapy.

The enzymes involved in the bacterial fatty acid biosynthetic pathway, the fatty acid synthase system, are attractive targets for the design of new antibacterial agents [6–9]. Fatty acid biosynthesis in bacteria is catalyzed by a set of distinct, monofunctional enzymes collectively known as the type II FAS (FASII). These enzymes differ significantly from the type I FAS (FASI) in mammals, in which all of the enzymatic activities are encoded in one or two multifunctional polypeptides. This distinctive difference in the FAS molecular organization between most bacteria and mammals makes possible the design of specific inhibitors of increased selectivity and lower

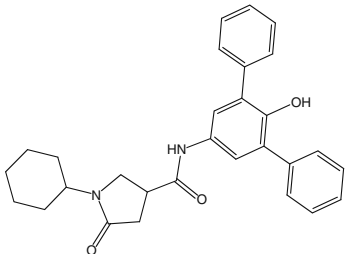
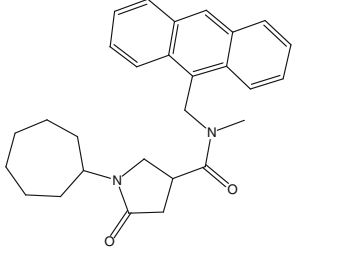
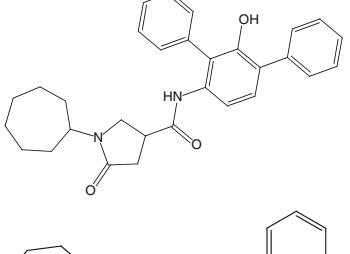
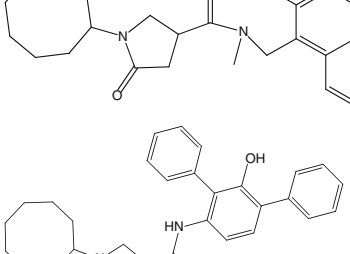
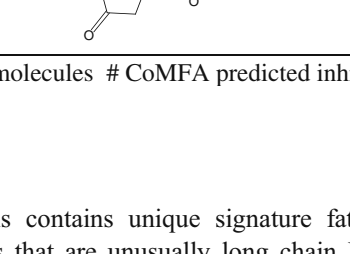
A. Kumar · M. I. Siddiqi (✉)
Molecular and Structural Biology Division,
Central Drug Research Institute,
Lucknow 226 001, India
e-mail: imsiddiqi@yahoo.com

Table 1 Structures and activities of pyrrolidine carboxamides used in CoMFA study

Serial Number	R1	R2	IC ₅₀	-logIC ₅₀	pIC ₅₀ [#]	Residual Value
						
1	H	H	10.66 ± 0.51	4.972	5.051	-0.079
2	H	2-COOMe	34.88 ± 2.06	4.457	4.618	-0.161
3*	H	3-Br	0.89 ± 0.05	6.05	5.880	0.170
4	H	4-Br	28.02 ± 4.29	4.552	4.740	-0.188
5	H	3-Cl	1.35 ± 0.05	5.869	5.864	0.005
6	H	4-I	14.50 ± 0.79	4.838	4.682	0.156
7	H	3-Me	16.79 ± 0.54	4.774	4.867	-0.093
8	H	3-CF ₃	3.51 ± 0.09	5.454	5.312	0.142
9	H	3-NO ₂	10.59 ± 0.48	4.975	4.985	-0.01
10	H	3-CH(CH ₃) ₂	5.55 ± 0.21	5.255	5.226	0.029
11	H	4-Ac	73.58 ± 9.97	4.133	4.091	0.042
12	2-Cl	4-Cl	56.02 ± 10.23	4.251	4.325	-0.074
13	2-Cl	5-Cl	56.50 ± 11.09	4.247	4.315	-0.068
14	2-Me	5-Cl	0.97 ± 0.03	6.013	5.953	0.060
15	3-Me	4-Br	37.41 ± 1.76	5.22	5.016	0.204
16*	2-Me	5-Me	10.05 ± 0.33	4.997	5.232	-0.235
17	3-Me	5-Me	3.14 ± 0.12	5.503	5.159	0.344
18	2-Me	3-Cl	23.12 ± 1.00	4.636	4.723	-0.087
19	2-Me	4-NO ₂	31.37 ± 1.45	4.503	4.370	0.133
20	3-F	5-F	1.49 ± 0.05	5.826	5.830	-0.004
21	3-Cl	5-Cl	0.39 ± 0.01	6.408	6.059	0.349
22	3-Br	5-CF ₃	0.85 ± 0.05	6.07	6.001	0.069
23	3-OMe	5-CF ₃	1.30 ± 0.04	5.886	6.035	-0.149
24	3-CF ₃	5-CF ₃	3.67 ± 0.17	5.435	5.927	-0.492
25	2-OMe	5-Cl	1.60 ± 0.06	5.795	5.798	-0.003
26	3-Cl	4-F	14.83 ± 0.98	4.828	4.868	-0.040
27*			5.1	5.292	5.536	-0.244

28*		0.39 ± 0.01	6.408	6.458	-0.050
29*		0.41 ± 0.01	6.387	6.371	0.016
30		0.75 ± 0.04	6.124	6.208	-0.084
31		1.39 ± 0.02	5.856	5.624	0.232
32*		3.39 ± 0.10	5.469	5.247	0.222
33		4.47 ± 0.28	5.349	5.275	0.074
34		2.57 ± 0.17	5.59	5.817	-0.227

35				5.18 ± 0.34	5.285	5.182	0.103
36				6.41 ± 0.12	5.193	5.256	-0.063
37*				5.51 ± 0.22	5.258	5.227	0.031
38*	3-Cl	H		3.94 ± 0.34	5.4	5.640	-0.240
39*	3-Br	4-F		13.55 ± 0.85	4.53	4.843	-0.313
40	3-Br	H		29.23 ± 2.17	4.87	4.975	-0.105
41				0.845 ± 0.05	6.073	6.142	-0.069
42				0.46 ± 0.01	6.337	6.406	-0.069

43		0.14 ± 0.01	6.853	6.720	0.133
44		0.62 ± 0.05	6.207	6.278	-0.071
45		0.36 ± 0.03	6.443	6.435	0.008
46		0.32 ± 0.02	6.494	6.440	0.054
47*		1.29 ± 0.10	5.889	5.667	0.222

* Test set molecules # CoMFA predicted inhibitory activity

toxicity. *M. tuberculosis* contains unique signature fatty acids, the mycolic acids that are unusually long chain R-alkyl, β -hydroxy fatty acids of 60–90 carbons [10]. The TB-specific drugs isoniazid (isonicotinic acid hydrazide (INH)) and ethionamide have been shown to target the synthesis of these mycolic acids, which are central constituents of the mycobacterial cell wall. Among the enzymes involved in FASII, the NADH-dependent enoyl-ACP reductase encoded by the *Mycobacterium* gene *inhA* is a key catalyst in mycolic acid biosynthesis. Studies over the years have established that *InhA* is the primary molecular targets of INH, [11] the drug that for the past 40 years has been, and continues to be, the frontline agent for the treatment of TB. Thus, *InhA* inhibitors would be

promising candidates for the development of novel anti-tubercular agents. Here, we present the results of comparative molecular field analysis (CoMFA) calculations carried out on pyrrolidine carboxamides, reported to be selective inhibitors of mycobacterial Enoyl acyl carrier protein reductase. Partial least square (PLS) [12] based statistical analysis was carried out on aligned molecules to identify the correlation. The contour maps generated help in explaining the observed variation in activity for given structural difference in EACP reductase inhibitors. Important features observed in the developed model have been used to design new molecules using the program LeapFrog, which showed higher predictivity and binding energy when compared with existing systems.

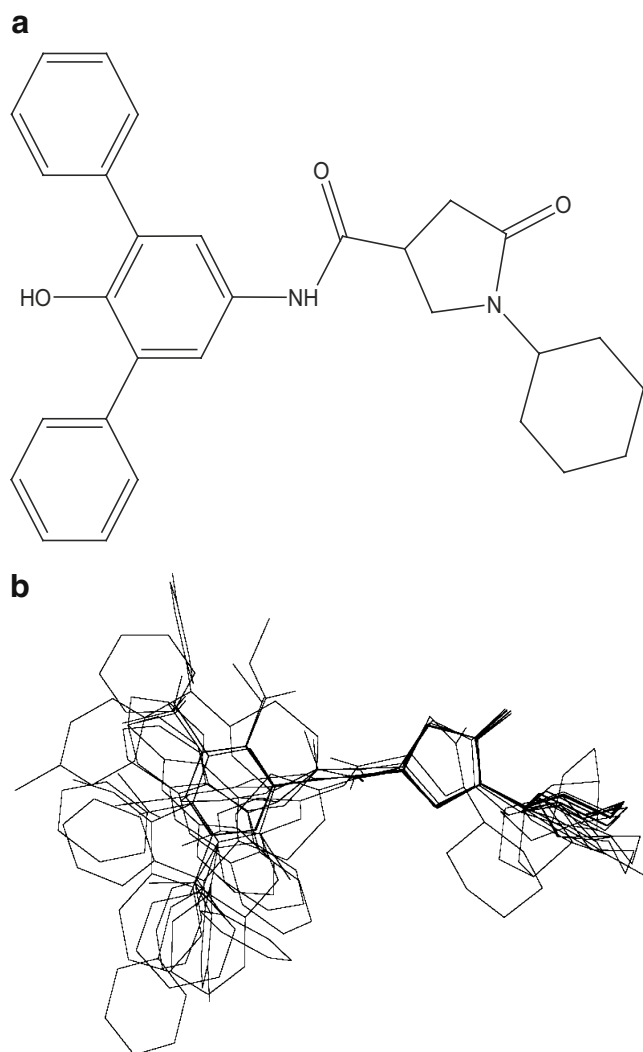


Fig. 1 (a) Template used for molecular alignment of pyrrolidine carboxamides (b) Molecular alignment

Materials and methods

Dataset

In vitro inhibitory activity data (IC_{50} μ M) of the Pyrrolidine Carboxamides on *Mycobacterium tuberculosis* EACP reductase, reported by Xin He et al. [13] was taken for the study. Forty seven molecules were selected for developing the model and the rest of the molecules whose IC_{50} values reported as >100 were not considered in this study. The structure of the compounds and their biological data is given in Table 1. The IC_{50} values were converted to the corresponding pIC_{50} ($-\log IC_{50}$) and used as dependent variables in CoMFA analysis. The pIC_{50} values span a range of 3 log units providing a broad and homogenous data set for CoMFA study. The CoMFA model was generated using a training set of 37 molecules. Predictive

power of the resulting model was evaluated using a test set of 10 molecules (Table 1 marked with *). The test compounds were selected manually such that the structural diversity and wide range of activity in the data set were included.

Molecular alignment

Structural alignment is one of the most sensitive parameters in CoMFA analysis. The accuracy of the prediction of CoMFA models and the reliability of the contour models depend strongly on the structural alignment of the molecules [14]. The molecular alignment was achieved by the Sybyl 7.1 routine database align. The most active compound 43 (Fig. 1a) was used as the alignment template, and the rest of the molecules were aligned on it by using the common substructure (Fig. 1b).

CoMFA studies

Steric and electrostatic interactions were calculated using the Tripos force field [15] with a distance-dependent dielectric constant at all interactions in a regularly spaced (2Å) grid taking a sp^3 carbon atom as steric probe and a $+1$ charge as electrostatic probe. The cutoff was set to 30 kcal/mol. With standard options for scaling of variables, the regression analysis was carried out using the full cross-validated partial least squares (PLS) [16] method (leave one out). The minimum sigma (column filtering) was set to

Table 2 Statistical results for CoMFA model

	CoMFA
PLS statistics	
q^{2a}	0.626
r^{2b}	0.953
S^c	0.170
F^d	124.474
Optimal components ^e	5
Field distribution %	
Steric	52.0
Electrostatic	48.0
$r^{2f}_{bootstrap}$	0.963
$S_{bootstrap}^g$	0.147
r^{2h}_{pred}	0.880
S_{pred}^i	0.199

a Cross-validated correlation coefficient

b Non-cross-validated correlation coefficient

c Standard error of estimate

d F test value

e Optimum number of components

f Predictive correlation coefficient

g Standard error of prediction

h Bootstrap correlation coefficient

i Standard error of Bootstrapping

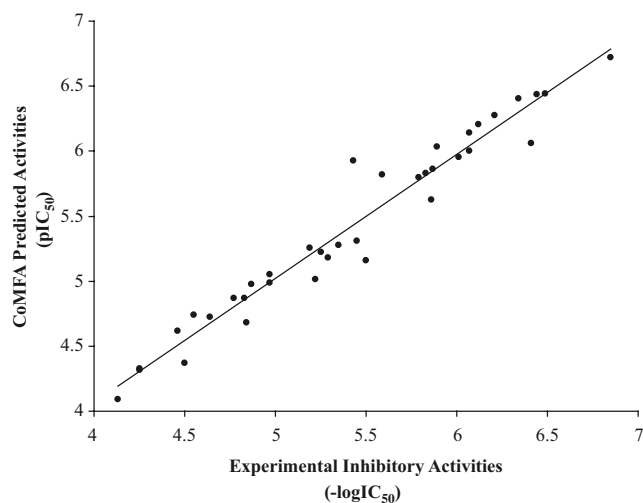


Fig. 2 Correlation between CoMFA predicted activities and experimental activities of training set compounds

2.0 kcal/mol to improve the signal to noise ratio by omitting those lattice points whose energy variation was below this threshold. The final model, non cross-validated conventional analysis was developed with the five optimum numbers of components to yield a non cross-validated r^2 value.

Partial least square (PLS) analysis

PLS method [16] was used to linearly correlate the CoMFA fields to biological activity values. The cross-validation was performed using the leave-one-out (LOO) method in which one compound is removed from the dataset and its activity is predicted using the model derived from the rest of the molecules in the dataset. Equal weights for CoMFA were assigned to steric and electrostatic fields using CoMFA STD scaling option. To speed up the analysis and reduce noise, a minimum column filter value of 2.0 kcal/mol was used for the cross-validation. Non-cross-validation was performed to calculate conventional r^2 using the same number of components. To further assess the robustness and statistical confidence of the derived models, bootstrapping analysis for 100 runs was performed [16] and [17]. Bootstrapping involves the generation of many new data sets from the original data set and is obtained by randomly choosing samples from the original data set. The statistical calculation is performed on each of these bootstrapping samplings. The difference between the parameters calculated from the original data set and the average of the parameters calculated from the many bootstrapping samplings is a measure of the bias of the original calculations. The entire cross-validated results were analyzed considering the fact that a value of q^2 above 0.3 indicates that probability of chance correlation is less than 5% [16].

De novo design of ligands using LeapFrog

LeapFrog, a *de novo* ligand design tool interfaced with Sybyl7.1 [18] was used to design new ligands using the CoMFA results. LeapFrog makes use of the CoMFA contours for the generation of a hypothetical cavity and then design new ligands based on the hypothetical cavity features. The results of PLS analysis described above and the region file of the contour was used for cavity generation calculations. New ligands were designed using OPTIMIZE mode of LeapFrog. Highly active compounds 43 and 46 were taken as templates to design new ligands. WEED step was performed immediately after the run of 100 moves which discards all ligands except the top n in binding score, where n was set to be 10 which is the default number of ligands as per the SYBYL tailor set-up. CROSSOVER, a genetic move for generating the best hybridizations among these diverse structural changes was also performed.

Hardware and software

InsightII 2000.1 [18] and Sybyl 7.1 [19] were used for molecular modeling on a SGI Origin 300 workstation equipped with 4 * 600 Mhz R12000 processors.

Result and discussion

CoMFA studies

CoMFA 3D-QSAR model was derived using previously reported Pyrrolidine Carboxamides as Enoyl acyl carrier protein inhibitors [13]. The chemical structures of mole-

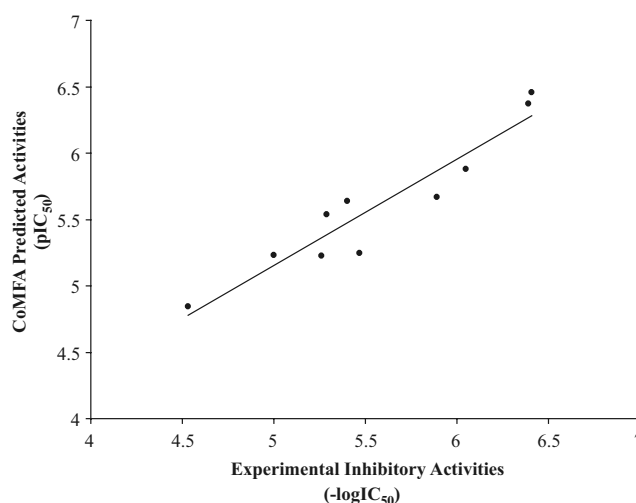


Fig. 3 Correlation between CoMFA predicted activities and experimental activities of test set compounds

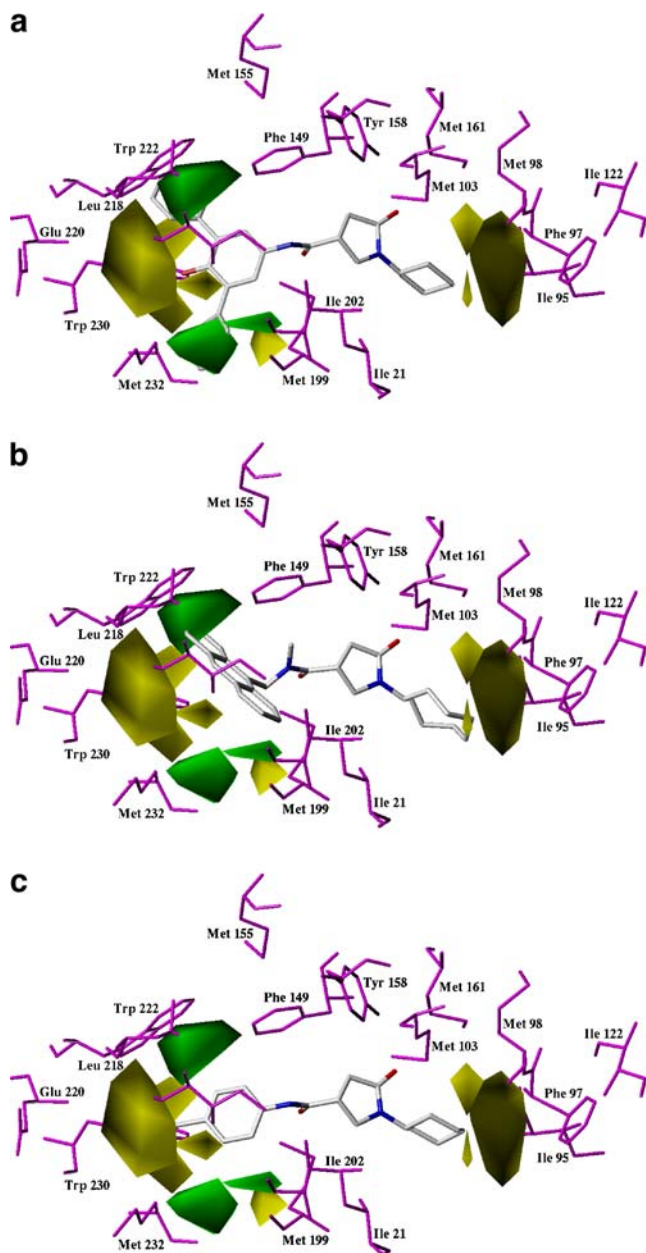


Fig. 4 CoMFA steric contour map with (a) compound 43 (b) compound 46 and (c) compound 11. Green color represents the region where steric bulk is favorable for increase in inhibitory activity and yellow color represents region where steric bulk is unfavorable

cules and their experimental IC_{50} values are shown in Table 1. Thirty seven compounds out of the total forty seven *Mycobacterium tuberculosis* enoyl acyl carrier protein inhibitors were used as training set and ten compounds were used as test set. PLS analysis was carried out for the training set and the results are listed in Table 2, which shows that a CoMFA model with a cross-validated q^2 of 0.626 for five components was obtained. The non cross-validated PLS analysis with the optimum components revealed a conventional r^2 value of 0.953, $F=124.474$ and

an estimated standard error of 0.170. The steric field descriptors explain 52% of the variance, while the electrostatic descriptors explain 48% of the variance. Bootstrap analysis for 100 runs was then carried out for further validation of the model by statistical sampling of the original data set to create new data sets. Thus, the difference in the parameters calculated from the original data and the average of the parameters calculated from the $N (=100)$ runs of bootstrapping sampling is a measure of the bias of the original calculation. This yielded higher $r^2_{\text{bootstrap}}$ value 0.963 for CoMFA and further supports the statistical validity of the developed models. The predicted activities for the inhibitors versus their experimental activities are listed in Table 1; the correlation between the predicted activities and the experimental activities is depicted in Fig. 2. Table 1 and Fig. 2 demonstrate that the predicted activities by the constructed CoMFA model are in good agreement with the experimental data, suggesting that the CoMFA model should have a satisfactory predictive ability.

Validation of 3D-QSAR models:

The ten manually selected compounds (Table 1) were used as testing set to verify the stability and predictive ability of the constructed CoMFA model. The predicted pIC_{50} with the QSAR model are in good agreement with the experimental data within a statistically tolerable error range, with a predicted correlation coefficient of $r_{\text{pred}}^2=0.880$ and 0.199 as the standard error of predictions (Table 1). The correlation between the CoMFA predicted activities and the experimental activities of the test set compounds are depicted in Fig. 3. The testing results indicate that the CoMFA model would be reliably used in the design of new EACP reductase inhibitors.

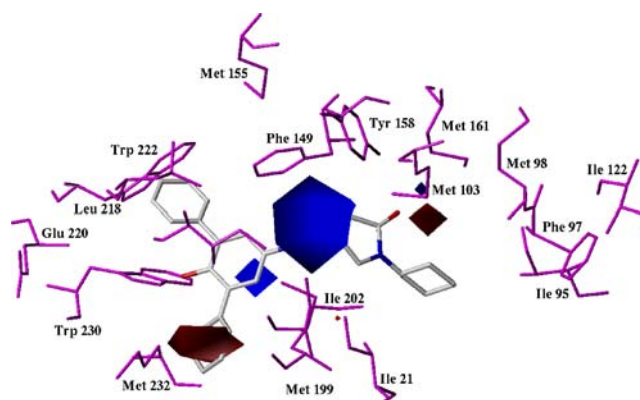
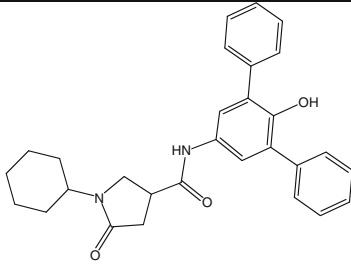
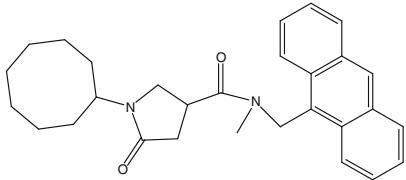
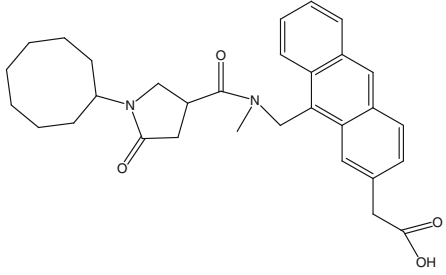
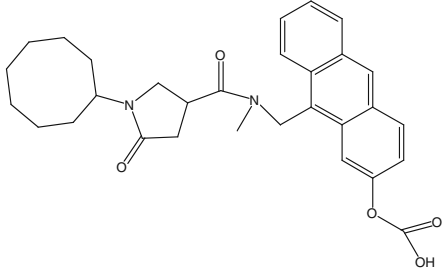
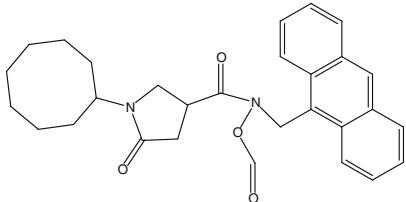
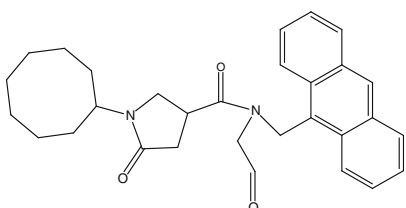
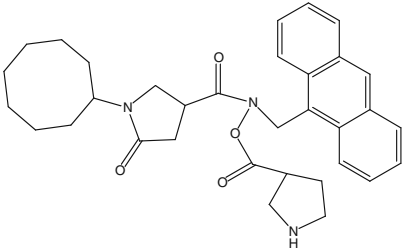
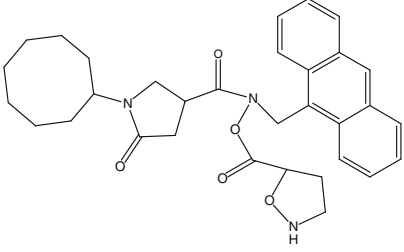
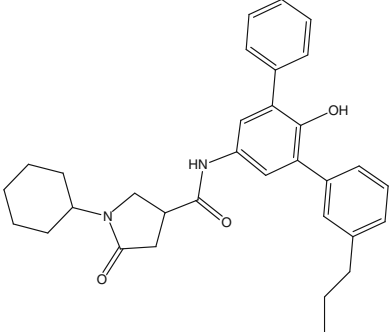
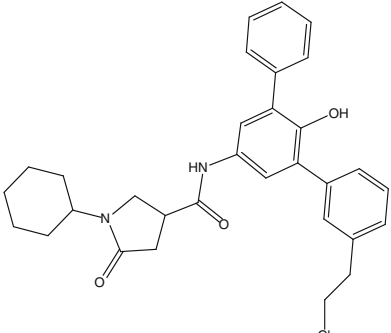
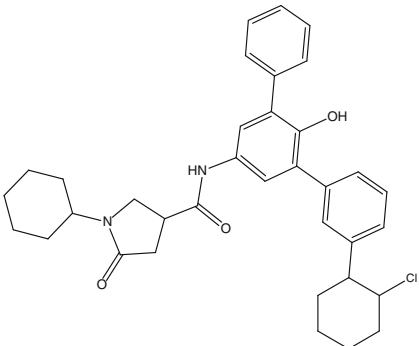


Fig. 5 CoMFA electrostatic contour map with compound 43. Blue color represents regions where an increased positive charge is favorable for inhibitory activity and red color represents regions where an increased negative charge is favorable for the activity

Table 3 Structure, Leapfrog binding energy and CoMFA predicted activities of the designed compounds

Compound	Structure	$-\log IC_{50}$	pIC_{50}	LeapFrog BE (kcal/mol)
43		6.853	6.720	-599.04
46		6.494	6.440	-574.88
ND1		-	6.646	-592.16
ND2		-	6.625	-597.63
ND3		-	7.013	-604.57
ND4		-	7.062	-642.76

ND5		-	7.001	-596.15
ND6		-	6.883	-804.72
ND7		-	7.010	-614.23
ND8		-	7.042	-626.21
ND9		-	7.085	-665.69

ND10		-	7.092	-645.45
ND11		-	7.348	-671.48
ND12		-	7.235	-672.53
ND13		-	7.121	-759.89

Contour analysis

The visualization of the results of the CoMFA model have been performed using the StDev*Coeff mapping option contoured by contribution. In order to investigate

the relationship between contours and ligand-receptor interaction, the contours were mapped onto the structure of EACP reductase, taken from the Protein Data Bank (2H7M) by superimposing the template ligand from the co-crystal structure onto the same ligand present in the CoMFA training set. The default level

of contour by contribution, 80 for favored region and 20 for disfavored region was set during contour analysis.

CoMFA contour maps

CoMFA steric and electrostatic contours are shown in Figs. 4 and 5. The steric interaction is represented by green (sterically favorable) and yellow (sterically unfavorable) contours, while electrostatic interaction is denoted by red (electronegative charge favorable) and blue (electropositive charge favorable) contours. A large green contour was found near one of the phenyl ring of compound 43 and anthracene ring of compound 46 indicating that bulky substituents were preferred in this region (Fig. 4a and b). This may be the reason why compounds with large aromatic substituents in this area, e.g., compounds 28–30 and 41–47 are more potent than molecules with small substituents, such as compounds 1–6, 12, 13 and 15–20. This sterically preferred area is located near hydrophobic amino acids such as Phe149, Leu218 and Trp222. Hence, more bulky aromatic substitutions of the inhibitors can interact better with the side chains of these residues via hydrophobic interactions. Another sterically favored green contour is located close to the other phenyl ring of compound 43. The phenyl ring of the most active compound, 43, is located near to this green region and therefore it exhibits higher potency than 46 which do not have functional groups extended to this area. The side chains of Ile202, Trp230 and Met232 are very close to this green contour. Four yellow contours are located around the acetyl group substituted at para position of the phenyl ring of compound 11 suggesting that small bulky groups are required to increase the activity. This is possibly a reason why, compound 11 is less potent as compared to the compounds without substituents at this position like compounds 1, 3, 5 and 20–25. The acetyl substituted phenyl ring of compound 11 overlapped with one of these four yellow contours suggesting that substituents here might be involved in steric clashes with Ile215 and Trp230; therefore, larger substituents in these regions reduce the activity. Figure 4 a and b also show one big and two small yellow contours located near the phenyl ring attached to pyrrolidine ring of compound 43, which indicates that steric bulk is disfavored for the activity in this area. Increasing the bulkiness of the substituent at this position, such as in case of compounds 44–47 decreases the inhibitory activity when compared with compound 43, probably because of increased steric hindrance due to Phe97 and Ile95 near these yellow contours.

The CoMFA electrostatic contour plot is displayed in Fig. 4c. Blue contours indicate that substituents should be electron deficient for high binding affinity and the red

contours represents the region favoring electron rich substituents. A big blue contour was found overlapping amide group of all the pyrrolidine carboxamide indicating that the presence of electron rich functionalities in this region may be necessary for the binding and hence for EACP reductase inhibition. A small red contour is also seen near the pyrrolidine oxygen which also confirms the presence of this moiety for EACP reductase inhibition. The presence of negatively charged environment at this position is favorable for the hydrogen bonding interactions with side chain oxygen of Tyr 158 and nicotinamide ribose of cofactor NAD (NAD not shown in figure for clarity). However, it was seen from the statistical analysis that the contribution of electrostatic component to the variance is smaller when compared with the steric component of CoMFA. These differences are also reflected in the CoMFA contour maps. A small red contour, region favorable for electron deficient substitution is found overlapping one of the phenyl rings of compound 43 indicating that the substitution of negatively charged groups at various position of the phenyl ring may enhance the activity. This negatively charged favored region was observed near Arg195 implying that electron rich groups may interact with side chain of Arg195 and therefore increase the inhibitory potencies of pyrrolidine carboxamides. (Fig. 5)

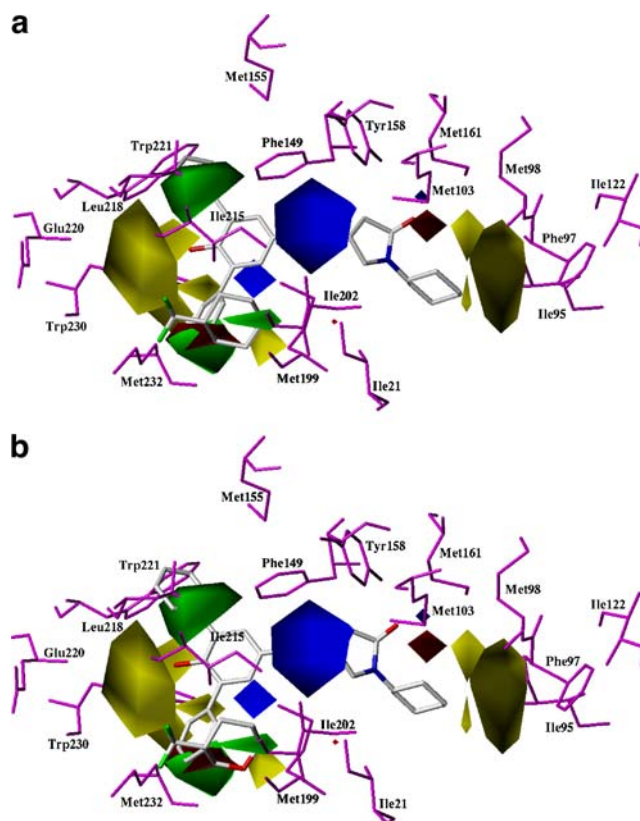


Fig. 6 Leapfrog designed molecule superimposed on CoMFA contour map (a) Compound ND11 and (b) Compound ND12

LeapFrog based *de novo* design of new molecules

The detailed contour analysis of CoMFA model enabled us to point out several structural requirements as mentioned above for the observed inhibitory activities. PLS analysis was used to design new ligands using *de novo* ligand generation program, LeapFrog. The OPTIMIZE mode of the LeapFrog was used for the optimization of the ligands. The highly active molecules 43 and 46 were subjected to OPTIMIZE mode for their improvement in binding energy and predicted activity. A total of 13 molecules were designed which show improved binding energy and CoMFA predicted inhibitory activity over the template molecules used for the designing. The structures of newly designed molecules along with their binding energies and CoMFA predicted inhibitory activities are shown in Table 3. In the case of pyrrolidine carboxamides there is a defined central core, which is common to all molecules. The aromatic substitution toward the amide linkage can be defined as region A, while substitution toward the pyrrolidine ring can be defined as region B. Structurally; the designed molecules differ from the reported molecules with addition of bulky substituents in region A and maintaining the similar steric bulk at region B. In some cases addition of substituents at the central core resulted in increased activity. Newly designed molecules were further validated by mapping these compounds onto the CoMFA contour maps. In Fig. 6a Trifluoromethyl substituted phenyl ring of Compound ND11 is going toward the sterically favorable green contour where bulky groups can interact via hydrophobic contacts with Ile 21, Met 199 and Ile 202. Designed compound ND11 exhibit improved LeapFrog binding energy of -671.48 kcal/mol and CoMFA predicted activity (pIC_{50}) of 7.348 over highly active template molecule (compound 43) with Leapfrog binding energy of -599.04 kcal/mol and $-\log IC_{50}$ of 6.853 (Table 3). Similarly in the case of ND12, the presence of a trifluoro tetrahydropyran substitution in the steric and negatively charged favorable region increases the activity (7.235) and binding energy (-672.53 kcal/mol) as compared to the template molecule 43, based on the CoMFA model (Fig. 6b and Table 3).

Conclusions

In this study 3D CoMFA QSAR analysis was used to predict the EACP reductase inhibitory activities of a set of pyrrolidine carboxamides. The 3D-QSAR model gave good statistical results in terms of q^2 and r^2 values. The CoMFA model provided the most significant correlation of steric

and electrostatic fields with the biological activities. The statistical significance and robustness of the 3D-QSAR model generated was confirmed using a test set. The effects of the steric and electrostatic fields around the aligned molecules on their activities were clarified by analyzing the CoMFA contour maps. Finally, Leapfrog was employed to design molecules based on the information derived from the CoMFA contour maps. A series of molecules designed by this approach are presented in this work. This study provides valuable results in search and rational design of more potent antitubercular agents.

Acknowledgements This manuscript is CDRI communication number 7455. This work was supported by the Council of Scientific and Industrial Research (CSIR) funded network project CMM0017- Drug Target development using *in silico* biology. Ashutosh Kumar thanks CSIR for fellowship.

References

1. World Health Organization (2005) Fact sheet on tuberculosis <http://www.who.int/mediacentre/factsheets/fs104/en/print.html>
2. Bloom BR, Murray CJ (1992) *Science* 257:1055–1064
3. Heym B, Honore N, Truffot-Pernot C, Banerjee A, Schurra C, Jacobs Jr WR, van Embden JD, Grosset JH, Cole ST (1994) *Lancet* 344:293–298
4. Perlman DC, ElSadr WM, Heifets LB, Nelson ET, Matts JP, Chirgwin K, Salomon N, Telzak EE, Klein O, Kreiswirth BN, Musser JM, Hafner R (1997) *AIDS* 11:1473–1478
5. Rattan A, Kalia A, Ahmad N (1998) *Emerging Infect Dis* 4:195–209
6. Campbell JW, Cronan JE Jr (2001) *Annu Rev Microbiol* 55:305–332
7. Heath RJ, Rock CO (2004) *Curr Opin Invest Drugs* 5:46–153
8. White SW, Zheng J, Zhang YM, Rock CO (2005) *Annu Rev Biochem* 74:791–831
9. Zhang YM, Lu YJ, Rock CO (2004) *Lipids* 39:1055–1060
10. Takayama K, Wang C, Besra GS (2005) *Clin Microbiol Rev* 18:81–101
11. Banerjee A, Dubnau E, Quemard A, Balasubramanian V, Um KS, Wilson T, Collins D, de Lisle G, Jacobs WR Jr (1994) *Science* 263:227–230
12. Wold S, Johansson A, Cochi M (1993) 3D QSAR in drug design: theory, methods and applications. In: PLS-Partial Least Squares Projection to Latent Structures. ESCOM, Lieden, pp 523–550
13. Xin H, Alian A, Stroud R, de Montellano PRO (2006) *J Med Chem* 49:6308–6323
14. Cho SJ, Tropsha A (1995) *J Med Chem* 38:1060–1066
15. Clark MC, Cramer RD III, van Opden Bosch N (1989) *J Comput Chem* 10:982–1012
16. Cramer RD, Bunce JD, Patterson DE (1988) *Quant Struct Act Relat* 7:18–25
17. Clark M, Cramer RD III, Jones DM, Patterson DE, Simeroth PE (1990) *Tetrahedron Comput Methodol* 3:47–59
18. SYBYL Molecular Modeling System Version 7.1 (2005), Tripos Inc., St. Louis, MO
19. Insight II 2000.1 Program (2000) Accelrys, San Diego, CA